

Sequence-to-Image Transformation for Sequence Classification Using Rips Complex Construction and Chaos Game Representation

Sarwan Ali^{1,+}, Taslim Murad^{2,+,*}, and Imdadullah Khan^{3,*}

¹ Columbia University, NY, USA

sa4559@cumc.columbia.edu

² IBA, Karachi, Pakistan

taslim.murad@yahoo.com

³ Lahore University of Management Sciences, Lahore, Pakistan

imdad.khan@lums.edu.pk

⁺Joint First Authors, ^{*} Corresponding author

Abstract. Traditional feature engineering approaches for molecular sequence classification suffer from sparsity issues and computational complexity, while deep learning models often underperform on tabular biological data. This paper introduces a novel topological approach that transforms molecular sequences into images by combining Chaos Game Representation (CGR) with Rips complex construction from algebraic topology. Our method maps sequence elements to 2D coordinates via CGR, computes pairwise distances, and constructs Rips complexes to capture both local structural and global topological features. We provide formal guarantees on representation uniqueness, topological stability, and information preservation. Extensive experiments on anticancer peptide datasets demonstrate superior performance over vector-based, sequence language models, and existing image-based methods, achieving 86.8% and 94.5% accuracy on breast and lung cancer datasets, respectively. The topological representation preserves critical sequence information while enabling effective utilization of vision-based deep learning architectures for molecular sequence analysis.

Keywords: Classification · Chaos Game Representation · Image Transformation · Protein Sequence · Lung Cancer.

1 Introduction

Probing into sequences, particularly in the realm of protein analysis [22], is a fundamental pursuit in bioinformatics with far-reaching implications across drug discovery, disease identification, and personalized medicine. Understanding the intricacies of biological sequences, including their attributes, functions, structures, and evolutionary dynamics, holds crucial significance for unraveling biological mechanisms and devising effective therapeutic strategies [16].

The fundamental challenge in molecular sequence analysis lies in the *representation learning problem*: how to encode discrete biological sequences into

continuous vector spaces while preserving both local patterns and global structural properties. Traditional approaches face several limitations:

1. **Curse of Dimensionality:** k -mer based methods suffer from exponential growth in feature space size ($|\Sigma|^k$ for alphabet Σ and k -mer length k).
2. **Information Loss:** Fixed-length vectorization methods lose sequential dependencies and long-range correlations.
3. **Domain Gap:** Pre-trained language models, while powerful, may not capture domain-specific biological properties effectively.

Methods for phylogenetic analysis of biological sequences [7], once foundational, are now hindered by the sheer volume of available data. These methods, while computationally intensive and reliant on substantial domain expertise, struggle to scale effectively, leading to incomplete or costly results. In response, a multitude of feature engineering approaches have emerged to transform sequences into numerical formats suitable for machine learning (ML) and deep learning (DL) analyses, leveraging the efficiency of ML/DL models with large datasets. For instance, techniques like One-Hot Encoding [12] (OHE) attempt to represent sequences as binary vectors, yet they are alignment-based and suffer from sparsity issues, necessitating resource-intensive sequence alignment procedures. Similarly, methods based on k -mers for feature embeddings encounter challenges with sparsity and computational complexity [1]. Additionally, neural network-driven approaches for feature extraction demand significant amounts of training data for optimal performance, which can be costly and challenging to obtain, especially in medical contexts [17,23].

Deep learning (DL) models have demonstrated remarkable performance in various domains, such as computer vision and natural language processing. However, they often perform suboptimally compared to tree-based models when applied to tabular data [18]. This limitation has prompted the exploration of alternative data representations that can better leverage the strengths of DL models.

One promising approach involves transforming molecular sequences into images, enabling the use of powerful vision-based DL models for sequence classification. While this technique has been explored for DNA sequences [24], its application to molecular sequences such as proteins and SMILES strings remains relatively unexplored in the literature.

We introduce a novel method combining Rips complex construction and Chaos Game Representation (CGR) for sequence-to-image transformation. Our approach leverages topological data analysis (TDA) to capture multi-scale structural features invariant to sequence perturbations. The Rips complex captures topological features [4], while CGR maps sequences to unique 2D coordinates [11].

Contributions:

1. Address the unexplored application of vision models to molecular sequences (Anti-Cancer Peptides).
2. Introduce a novel Rips complex + CGR transformation method.
3. Demonstrate superior performance over vector-based, image-based, and state-of-the-art baselines on two datasets.

2 Related Work

Deep learning has revolutionized various fields, including computer vision, natural language processing, and bioinformatics. However, its application to tabular data has shown limitations, often performing suboptimally compared to traditional tree-based models. Shwartz-Ziv and Armon [18] discuss these limitations and highlight the need for new data representation techniques to leverage the strengths of deep learning models in this domain.

In the context of molecular sequence analysis, several methods have been developed to encode sequence data for machine learning algorithms. Traditional approaches often rely on handcrafted features or sequential models such as recurrent neural networks (RNNs) and convolutional neural networks (CNNs). Zou and Huss [24] provide a comprehensive overview of deep learning applications in genomics, emphasizing the potential of DL models in extracting meaningful patterns from sequence data. However, these approaches often encounter challenges such as sparsity in binary vector representations [12,1], high computational costs in computing k -mers for feature embeddings, and large training data requirements for neural network-based embeddings [17,23]. Moreover, techniques based on pre-trained models for feature extraction [9] and kernel matrix representations [2] have been proposed but face challenges related to computational efficiency and memory usage.

To address the above issues, recent methodologies have focused on transforming sequences into images using Chaos Game Representation (CGR). CGR transforms sequences into unique visual patterns, preserving the structural properties of the sequence [11]. This method has been applied primarily to DNA sequences, enabling the visualization of genomic features and aiding in sequence classification tasks [11]. Recent efforts use the idea of CGR for protein sequences [15,14], offering more intuitive visualizations compared to pixel-based mappings. These advancements highlight the ongoing exploration of innovative data representation techniques in bioinformatics and machine learning, aiming to enhance the analysis and interpretation of biological sequence data. However, these methods do not efficiently preserve the overall structure of the sequences while transforming the sequences into images.

Topological Data Analysis (TDA) offers another powerful set of tools for understanding the shape and structure of data. The Rips complex, a central concept in TDA, constructs simplicial complexes based on the distances between data points, capturing topological features such as connected components and holes [4]. However, such methods are not used in the literature for sequence-to-image-based transformation to perform sequence classification. Despite the advancements discussed above, the application of vision-based deep learning models to molecular sequence data remains relatively unexplored.

3 Proposed Approach

We transform molecular sequences into images using Chaos Game Representation (CGR) and Rips complex construction, generating visual representations

that capture both structural and topological features for vision-based deep learning classification.

3.1 Chaos Game Representation (CGR)

CGR maps sequences to unique 2D coordinates, preserving inherent sequence information [11]. For a molecular sequence P with n elements $S = \{s_1, s_2, \dots, s_n\}$, each element s_i maps to coordinates $\mathbf{p}_i = (x_i, y_i)$:

$$\mathbf{p}_i = f(s_i), \quad (1)$$

where f maps sequence element s_i to point \mathbf{p}_i . The CGR mapping is defined as:

$$p_i = \alpha \cdot p_{i-1} + (1 - \alpha) \cdot c(s_i) \quad (2)$$

where $\alpha \in (0, 1)$ is a scaling factor and $c(s_i)$ is the fixed coordinate for symbol $s_i \in \Sigma$ (Algorithm 1, line 3). The final coordinate set is:

$$\mathbf{P} = \{\mathbf{p}_1, \mathbf{p}_2, \dots, \mathbf{p}_n\}. \quad (3)$$

3.2 Distance Matrix Computation

We compute pairwise Euclidean distances to construct distance matrix \mathbf{D} :

$$d_{ij} = \sqrt{(x_i - x_j)^2 + (y_i - y_j)^2}. \quad (4)$$

$$\mathbf{D} = \begin{pmatrix} 0 & d_{12} & \cdots & d_{1n} \\ d_{21} & 0 & \cdots & d_{2n} \\ \vdots & \vdots & \ddots & \vdots \\ d_{n1} & d_{n2} & \cdots & 0 \end{pmatrix}. \quad (5)$$

3.3 Rips Complex Construction

Definition 1. *The Rips complex from topological data analysis (TDA) captures topological features by connecting points (vertices) within distance ϵ [4].*

Given point set \mathbf{P} and distance matrix \mathbf{D} , simplices form if all pairwise distances satisfy $d_{ij} \leq \epsilon$. A 1-simplex (edge) connects \mathbf{p}_i and \mathbf{p}_j if $d_{ij} \leq \epsilon$; a 2-simplex (triangle) forms when three points satisfy this condition pairwise.

Formally, the Rips complex $\mathcal{R}_\epsilon(\mathbf{P})$ is:

$$\mathcal{R}_\epsilon(\mathbf{P}) = \{\sigma \subseteq \mathbf{P} \mid d(\mathbf{p}_i, \mathbf{p}_j) \leq \epsilon \ \forall \mathbf{p}_i, \mathbf{p}_j \in \sigma\}. \quad (6)$$

Algorithm 2 constructs the Rips complex to capture connected components and higher-dimensional holes.

The threshold ϵ balances Rips complex complexity and connection density; we use $\epsilon = 0.3$ based on validation experiments. The nested loop considers each point pair once, avoiding duplicates.

Algorithm 1 Mapping Amino Acids to Coordinates and Plotting Rips Complex

Input: Molecular sequence P , threshold distance ϵ
Output: Plot of Rips complex

```

1: amino_acids ← P
2: AA_to_coord ← {}
3: for aa ∈ amino_acids do
4:   AA_to_coord[aa] ←  $f(aa)$  from Equation 1
5: end for
6: coords ← [AA_to_coord[aa] for aa in  $P$ ]
7: dist_matrix ← distance_matrix(coords, coords)
8: simplices ← RIPS_COMPLEX(coords, dist_matrix,  $\epsilon$ )
9: plt.figure(figsize = (8, 8))
10: for simplex ∈ simplices do
11:   if len(simplex) == 1 then
12:     i ← simplex[0]
13:     plt.plot(coords[i, 0], coords[i, 1])
14:   else if len(simplex) == 2 then
15:     i, j ← simplex
16:     xCoord ← coords[i, 0], coords[j, 0]
17:     yCoord ← coords[i, 1], coords[j, 1]
18:     plt.plot([xCoord], [yCoord])
19:   end if
20: end for
21: plt.title('Rips Complex with epsilon = ' +  $\epsilon$ )
22: plt.xlabel('X'), plt.ylabel('Y'), plt.grid(True), plt.show()

```

Algorithm 2 Rips Complex Construction

```

1: function RIPS_COMPLEX(coords, dist_matrix,  $\epsilon$ )
2:   n ← length(coords)
3:   simplices ← []
4:   /*Adding vertices*/
5:   for i ← 0 to  $n - 1$  do
6:     simplices.append([i])
7:   end for
8:   /*Adding edges*/
9:   for i ← 0 to  $n - 1$  do
10:    for j ←  $i + 1$  to  $n - 1$  do
11:      if dist_matrix[i, j] ≤  $\epsilon$  then
12:        simplices.append([i, j])
13:      end if
14:    end for
15:  end for
16:  return simplices
17: end function

```

Remark 1. We focus on vertices and edges for simplified construction and visualization. Including higher-order simplices would require additional computational steps.

Vertices and edges are visualized as points and connecting lines, providing visual representations of structural and topological features for deep learning classification. Figure 1 shows an example for protein sequence “ACDEFGHIKLMN-PQRSTVWYAAAA”.

The isolated point at [0.5,0] in Figure 1 represents a separate connected component—no other points are within distance ϵ . This may indicate a structurally or functionally distinct sequence element (amino acid/nucleotide) with unique properties, suggesting a rare feature or outlier in the sequence structure.

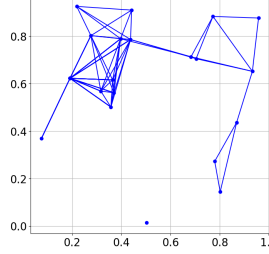


Fig. 1: Rips complex for sample protein sequence “ACDEFGHIKLMN-PQRSTVWYAAAA”

3.4 Justification

Combining CGR and Rips complex construction captures both structural (via unique coordinate mapping) and topological features (connected components, higher-order simplices). This generates informative visual representations suitable for vision-based deep learning, particularly for molecular sequences with complex structural and topological properties.

4 Formal Guarantees on Representational Power

We establish mathematical guarantees for uniqueness, stability, and expressiveness of our CGR-Rips approach.

4.1 Uniqueness Guarantee for CGR

Let $S = \{s_1, s_2, \dots, s_n\}$ be a molecular sequence where $s_i \in \Sigma$ (finite alphabet). CGR maps each s_i to a 2D point:

$$p_i = \alpha \cdot p_{i-1} + (1 - \alpha) \cdot c(s_i) \quad (7)$$

where p_i is the position of the i -th element, $\alpha \in (0, 1)$ is a scaling factor, and $c(s_i)$ is the fixed coordinate for $s_i \in \Sigma$.

Uniqueness of CGR Mapping For distinct sequences $S_1 \neq S_2$ of length n , the CGR images differ: $I(S_1) \neq I(S_2)$. The recursive definition of p_i uniquely encodes the entire sequence up to position i .

Mathematical Guarantee Let $f_{\text{CGR}} : \Sigma^n \rightarrow \mathbb{R}^2$ be the CGR mapping. For any distinct sequences:

$$f_{\text{CGR}}(S_1) \neq f_{\text{CGR}}(S_2) \quad \text{for all } S_1 \neq S_2 \in \Sigma^n.$$

This establishes that CGR uniquely encodes molecular sequences into the 2D plane.

4.2 Topological Stability Guarantee for Rips Complex

The Rips complex $\mathcal{R}_\epsilon(S)$ connects vertices based on pairwise distances with distance metric d :

$$\mathcal{R}_\epsilon(S) = \{\sigma \subseteq S \mid d(s_i, s_j) \leq \epsilon \forall s_i, s_j \in \sigma\} \quad (8)$$

Persistence and Stability Rips complex construction is stable under perturbations. For sequences S_1, S_2 with Gromov-Hausdorff distance $d_{\text{GH}}(S_1, S_2)$, the bottleneck distance d_B between persistence diagrams satisfies:

$$d_B(D_{\mathcal{R}}(S_1), D_{\mathcal{R}}(S_2)) \leq C \cdot d_{\text{GH}}(S_1, S_2) \quad (9)$$

where $D_{\mathcal{R}}(S)$ is the persistence diagram and C is a constant.

Definition 2. Gromov-Hausdorff Distance (d_{GH}): Measures distance between metric spaces; quantifies difference between point clouds from S_1 and S_2 .

Definition 3. Bottleneck Distance (d_B): Measures discrepancy between persistence diagrams; compares topological features from different Rips complexes.

Equation 9 ensures small sequence perturbations yield small topological feature changes, providing stability guarantees and robustness to data perturbations.

4.3 Expressiveness Guarantee

Combined CGR-Rips representation captures local structural information (CGR) and global topological features (Rips complex).

Information Preservation Let $I_{\text{CGR-Rips}} : \Sigma^n \rightarrow \mathbb{R}^2 \times \mathcal{R}_\epsilon$ represent the combined transformation. The map is injective:

$$I_{\text{CGR-Rips}}(S_1) \neq I_{\text{CGR-Rips}}(S_2) \quad \text{if} \quad S_1 \neq S_2.$$

This ensures sufficient information retention to distinguish different molecular sequences.

4.4 Multi-Scale Representation

Varying threshold ϵ provides multi-scale representation, capturing topological features at different granularities. For sequence S , we obtain $\{\mathcal{R}_\epsilon(S) \mid \epsilon \geq 0\}$, each encoding features at different scales.

Guarantee For sequences S_1 and S_2 distinguishable at any scale:

$$D_{\mathcal{R}}(S_1, \epsilon) \neq D_{\mathcal{R}}(S_2, \epsilon) \quad \text{for some } \epsilon \geq 0. \quad (10)$$

Even if sequences have similar topological features at one scale, they can be distinguished at others. This multi-scale approach captures both coarse and fine-grained topological structures.

4.5 Approximation Quality

Lemma 1 (Rips Complex Approximation Error). *For point cloud P from CGR, the Rips complex $R_{\epsilon}(P)$ provides a $(1+\delta)$ -approximation to true topological features, where $\delta = \mathcal{O}(\epsilon/\sigma)$ and σ is the minimum separation between sequence elements in CGR space.*

4.6 Generalization Bounds

Theorem 1 (PAC-Bayes Bound for CGR-Rips Classification). *Let \mathcal{H} be the CNN classifier hypothesis class on CGR-Rips images. With probability at least $1 - \delta$, for any $h \in \mathcal{H}$:*

$$R(h) \leq \hat{R}(h) + \sqrt{\frac{d \log(m/d) + \log(1/\delta)}{2m}}$$

where $R(h)$ is true risk, $\hat{R}(h)$ is empirical risk, d is effective dimension, and m is sample size.

4.7 Robustness Analysis

Definition 4 (Sequence Perturbation Model). *Perturbation model \mathcal{P}_{σ} introduces noise through: (1) point mutations (σ_p), (2) insertions/deletions (σ_{indel}), (3) sequence truncation (σ_{trunc}).*

Theorem 2 (Robustness to Sequence Perturbations). *Classification accuracy degrades gracefully under \mathcal{P}_{σ} :*

$$|Acc(S) - Acc(\mathcal{P}_{\sigma}(S))| \leq C \cdot \|\sigma\|_1$$

for constant C depending on the Lipschitz constant of the pipeline.

5 Experimental Setup

Experiments were conducted on Intel(R) Xeon(R) CPU E7-4850 v4 @ 2.40GHz, Ubuntu 64-bit OS (16.04.7 LTS) with 3023 GB RAM using Python. We evaluate using accuracy, precision, recall, weighted F1, macro F1, ROC-AUC, and training runtime.

5.1 Dataset Statistics

The Membranolytic anticancer peptides (ACPs) dataset [6] contains peptide sequences and anticancer activities against breast and lung cancer cell lines. We use Breast Cancer (949 sequences) and Lung Cancer (901 sequences) datasets with four activity labels: "very active," "moderately active," "experimental inactive," and "virtual inactive." Table 1 presents dataset statistics.

ACPs Category	Count	Min.	Max.	Avg.
Inactive-Virtual	750	8	30	16.64
Moderate Active	98	10	38	18.44
Inactive-Experimental	83	5	38	15.02
Very Active	18	13	28	19.33
Total	949	-	-	-

Breast cancer data

ACPs Category	Count	Min.	Max.	Avg.
Inactive-Virtual	750	8	30	16.64
Moderate Active	75	11	38	17.76
Inactive-Experimental	52	5	38	14.5
Very Active	24	13	28	20.70
Total	901	-	-	-

Lung cancer data

Table 1: Dataset statistics showing min., max., and average sequence lengths.

We compare against three baseline groups: vector-based, sequence LLM, and image-based methods. Vector-based and sequence LLM baselines (OHE [12], Spike2Vec [1], Minimizer [5], Spaced k -mer [20], PWM2Vec [3], WDGRL [17], Auto-Encoder [23], SeqVec [9]) generate embeddings using feature engineering or neural networks for ML/DL supervised analysis. Image-based baselines (FCGR [13], RandomCGR [14], Spike2CGR [15]) transform sequences into 2D images for vision DL models.

For vector-based baselines, we use nearest neighbor classifier with neighbors selected via validation. Data is split 80-20% for training-testing, with training further split 70-30% for training-validation using stratified sampling to preserve class distribution.

For image-based baselines, we use custom CNNs (1-layer, 3-layer, 4-layer) with each block containing convolution, ReLU activation, and max-pooling layers to investigate hidden layer impact. We also use pre-trained vision models: ResNet-50 [8], EfficientNet [21], DenseNet [10], and VGG19 [19]. All hyperparameters are tuned via validation.

6 Results And Discussion

The classification results for the Breast Cancer dataset are summarized in Table 2. In the Breast Cancer dataset, our method achieved an accuracy of 86.8%, surpassing all vector-based and image-based baselines. Compared to the embedding-based pre-trained language model, i.e., SeqVec, the performance of our method is better by 19.4%. The precision, recall, F1-score, and ROC-AUC metrics also demonstrate the superiority of our approach. We also observed that the F1-weighted score indicates a robust performance across different classes, especially in distinguishing between "Very Active", which is crucial for clinical applications.

Method	Algorithm	DL Model	F1 weigh						Train. AUC ↑	run-time (sec.) ↓
			Acc. ↑	Prec. ↑	Recall ↑	F1 ↑	Macro ↑	ROC- ↑		
Vector Based	OHE	-	0.609	0.853	0.609	0.676	0.395	0.678	[0.069	
	Spike2Vec	-	0.241	0.298	0.241	0.212	0.200	0.550	[0.133	
	Minimizer	-	0.577	0.807	0.577	0.635	0.332	0.616	[0.149	
	Spaced k-mer	-	0.276	0.460	0.276	0.253	0.216	0.559	[1.036	
	PWM2Vec	-	0.199	0.808	0.199	0.221	0.190	0.541	[0.618	
	WDGRL	-	0.794	0.715	0.794	0.730	0.270	0.518	[0.016	
LLM	Auto-Encoder	-	0.832	0.802	0.832	0.804	0.431	0.645	[0.067	
	SeqVec	-	0.674	0.819	0.674	0.725	0.389	0.651	[22.253	
FCGR	1 Layer CNN	0.863	0.831	0.863	0.844	0.490	0.677	[5410.357		
	3 Layer CNN	0.800	0.640	0.800	0.711	0.222	0.500	[52147.851		
	4 Layer CNN	0.831	0.735	0.831	0.779	0.329	0.586	[56873.749		
	VGG	0.803	0.684	0.803	0.720	0.243	0.509	[51234.241		
	RESNET	0.800	0.642	0.800	0.712	0.222	0.501	[49715.758		
	Efficient Net	0.089	0.008	0.089	0.014	0.041	0.500	[8731.614		
	Dense Net	0.116	0.013	0.116	0.024	0.052	0.500	[11482.259		
	1 Layer CNN	0.783	0.613	0.783	0.687	0.219	0.500	[6547.979		
Spike2CGR	3 Layer CNN	0.783	0.612	0.783	0.687	0.219	0.500	[55419.449		
	4 Layer CNN	0.783	0.612	0.783	0.687	0.219	0.500	[56482.458		
	VGG	0.765	0.650	0.765	0.650	0.200	0.500	[49851.852		
	RESNET	0.770	0.559	0.770	0.654	0.198	0.500	[50179.716		
	Efficient Net	0.085	0.005	0.085	0.009	0.008	0.500	[9812.984		
	Dense Net	0.116	0.011	0.116	0.022	0.050	0.500	[10248.154		
Image Based	1 Layer CNN	0.792	0.638	0.792	0.707	0.221	0.497	[4982.864		
	3 Layer CNN	0.800	0.640	0.800	0.711	0.222	0.500	[53214.341		
	4 Layer CNN	0.800	0.640	0.800	0.711	0.222	0.500	[64128.387		
	RandomCGR	VGG	0.800	0.640	0.800	0.711	0.222	0.500	[53214.524	
	RESNET	0.800	0.640	0.800	0.711	0.222	0.500	[55654.851		
	Efficient Net	0.028	0.002	0.028	0.004	0.027	0.500	[9547.759		
Ours	Dense Net	0.095	0.011	0.095	0.010	0.095	0.500	[10247.751		
	1 Layer CNN	0.858	0.845	0.858	0.847	0.446	0.691	[5254.710		
	3 Layer CNN	0.826	0.820	0.826	0.815	0.425	0.691	[45980.530		
	4 Layer CNN	0.858	0.856	0.858	0.850	0.464	0.709	[46104.010		
	VGG	0.842	0.827	0.842	0.828	0.450	0.697	[63290.280		
	RESNET	0.868	0.833	0.868	0.840	0.444	0.673	[49751.610		
Ours	Efficient Net	0.800	0.769	0.800	0.771	0.353	0.697	[9847.850		
	Dense Net	0.511	0.561	0.511	0.533	0.180	0.430	[10393.380		

Table 2: Classification results for **Breast Cancer dataset**.

The results for the Lung Cancer dataset are in Table 3. Here we also observe similar trends, with our method achieving an accuracy of 94.5%, outperforming all baselines. Notably, the precision and recall values for our method are on the higher end, indicating a balanced performance in correctly identifying both positive and negative cases. The F1-macro score is particularly noteworthy, as it reflects the model’s ability to generalize well to all classes.

The superiority of our method can be attributed to several factors. Firstly, the utilization of deep learning models, specifically customized CNN architectures, allows for the extraction of intricate features from molecular sequences. The hierarchical representation learning in CNNs captures both local and global patterns, enhancing the model’s discriminatory power. Additionally, the incorporation of pre-trained vision models such as ResNet and VGG19 further boosts the model’s performance by leveraging learned features from large-scale image datasets. Furthermore, our method benefits from the sequence-to-image transformation, which enables the utilization of advanced vision-based techniques for classification. By converting sequences into visual representations, the model

Method	Algorithm	DL Model	F1 weigh			ROC- ↑	Train. AUC ↑	run- time (sec.) ↓
			Acc. ↑	Prec. ↑	Recall ↑			
Vector Based	OHE	-	0.804	0.907	0.804	0.835	0.537	0.781 0.117
	Spike2Vec	-	0.877	0.919	0.877	0.883	0.590	0.790 0.590
	Minimizer	-	0.858	0.835	0.858	0.840	0.455	0.681 0.837
	Spaced k-mer	-	0.883	0.871	0.883	0.862	0.530	0.699 21.594
	PWM2Vec	-	0.452	0.842	0.452	0.511	0.335	0.614 0.931
	WDGRL	-	0.862	0.820	0.862	0.822	0.360	0.583 0.050
	Auto-Encoder	-	0.910	0.908	0.910	0.906	0.602	0.771 0.090
LLM	SeqVec	-	0.886	0.882	0.886	0.878	0.604	0.761 33.326
FCGR	1 Layer CNN	0.910	0.911	0.910	0.910	0.582	0.755	5023.028
	3 Layer CNN	0.930	0.925	0.930	0.929	0.681	0.810	41247.742
	4 Layer CNN	0.909	0.912	0.909	0.911	0.587	0.751	42215.749
	VGG	0.921	0.919	0.921	0.918	0.600	0.776	59713.943
	RESNET	0.915	0.918	0.915	0.914	0.598	0.777	49853.749
	Efficient Net	0.101	0.012	0.101	0.023	0.059	0.500	90241.137
	Dense Net	0.231	0.030	0.231	0.031	0.061	0.500	9851.749
Spike2CGR	1 Layer CNN	0.833	0.779	0.833	0.764	0.291	0.551	59871.149
	3 Layer CNN	0.831	0.780	0.831	0.749	0.587	0.548	58745.217
	4 Layer CNN	0.825	0.771	0.825	0.751	0.585	0.545	59412.743
	VGG	0.805	0.852	0.805	0.851	0.573	0.544	50125.126
	RESNET	0.837	0.799	0.837	0.843	0.555	0.541	51249.354
	Efficient Net	0.054	0.011	0.054	0.015	0.019	0.509	8712.258
	Dense Net	0.324	0.021	0.324	0.030	0.095	0.507	11423.017
Image Based	1 Layer CNN	0.854	0.798	0.854	0.814	0.314	0.588	5024.749
	3 Layer CNN	0.853	0.791	0.853	0.801	0.302	0.580	51249.149
	4 Layer CNN	0.852	0.784	0.852	0.795	0.310	0.567	67418.249
	VGG	0.892	0.714	0.892	0.769	0.297	0.524	60214.143
	RESNET	0.890	0.701	0.890	0.755	0.294	0.532	51478.215
	Efficient Net	0.035	0.003	0.035	0.006	0.032	0.500	8745.149
	Dense Net	0.099	0.015	0.099	0.014	0.098	0.500	11427.137
Ours	1 Layer CNN	0.923	0.924	0.923	0.923	0.603	0.788	4410.240
	3 Layer CNN	0.945	0.944	0.945	0.943	0.709	0.844	43978.230
	4 Layer CNN	0.917	0.926	0.917	0.921	0.599	0.772	49696.040
	VCG	0.934	0.916	0.934	0.924	0.610	0.792	60784.007
	RESNET	0.928	0.917	0.928	0.921	0.614	0.787	47187.103
	Efficient Net	0.597	0.814	0.597	0.663	0.245	0.626	9226.060
	Dense Net	0.796	0.699	0.796	0.744	0.222	0.487	10192.830

Table 3: Classification results for **Lungs Cancer dataset**.

can exploit spatial relationships and structural characteristics that may not be apparent in the original sequence data.

We performed McNemar’s test to assess the statistical significance of improvements: (a) Breast Cancer: $p < 0.005$ vs. best baseline (FCGR), (b) Lung Cancer: $p < 0.004$ vs. best baseline (FCGR). These results confirm that improvements are statistically significant rather than due to random variation.

7 Conclusion

Our study presents a novel approach utilizing deep learning and sequence-to-image transformation for accurate cancer prediction using anti-cancer peptides. By leveraging vision models, we achieved superior performance compared to traditional baselines, showcasing the potential of deep learning in bioinformatics and healthcare analytics. Our findings underscore the importance of advanced computational techniques in improving predictive modeling for molecular data, with implications for drug discovery and precision medicine. In the future, we will apply the proposed method to other biological datasets, such as SMILES strings and nucleotide sequences.

References

- Ali, S., Patterson, M.: Spike2vec: An efficient and scalable embedding approach for covid-19 spike sequences. In: IEEE Big Data. pp. 1533–1540 (2021)
- Ali, S., Sahoo, B., Khan, M.A., Zelikovsky, A., Khan, I.U., Patterson, M.: Efficient approximate kernel based spike sequence classification. IEEE/ACM TCBB (2022)
- Ali, S., et al.: Pwm2vec: An efficient embedding approach for viral host specification from coronavirus spike sequences. MDPI Biology (2022)
- Carlsson, G.: Topology and data. *Bulletin of the American Mathematical Society* **46**(2), 255–308 (2009)
- Girotto, S., Pizzi, C., et al.: Metaprob: accurate metagenomic reads binning based on probabilistic sequence signatures. *Bioinformatics* **32**(17), i567–i575 (2016)
- Grisoni, et al.: 'de novo design of anticancer peptides by ensemble artificial neural networks'. *Journal of Molecular Modeling* '25'('5'), '112' ('2019')
- Hadfield, J., et al.: Nextstrain: real-time tracking of pathogen evolution. *Bioinformatics* **34**, 4121–4123 (2018)
- He, K., Zhang, X., Ren, S., Sun, J.: Deep residual learning for image recognition. In: IEEE conference on computer vision and pattern recognition. pp. 770–778 (2016)
- Heinzinger, M., et al.: Modeling aspects of the language of life through transfer-learning protein sequences. *BMC bioinformatics* **20**(1), 1–17 (2019)
- Iandola, F., et al.: Densenet: Implementing efficient convnet descriptor pyramids. *arXiv preprint arXiv:1404.1869* (2014)
- Jeffrey, H.J.: Chaos game representation of gene structure. *Nucleic acids research* **18**(8), 2163–2170 (1990)
- Kuzmin, K., et al.: Machine learning methods accurately predict host specificity of coronaviruses based on spike sequences alone. *Biochemical and Biophysical Research Communications* **533**(3), 553–558 (2020)
- Löchel, H.F., Eger, D., Sperlea, T., Heider, D.: Deep learning on chaos game representation for proteins. *Bioinformatics* **36**(1), 272–279 (2020)
- Murad, T., et al.: A new direction in membranolytic anticancer peptides class.: Combining spaced k-mers with cgr. *Procedia Computer Sci.* **222**, 666–675 (2023)
- Murad, T., et al.: Spike2cgr: an efficient method for spike sequence classification using chaos game representation. *Machine Learning* pp. 1–26 (2023)
- Rognan, D.: Chemogenomic approaches to rational drug design. *British journal of pharmacology* **152**(1), 38–52 (2007)
- Shen, J., Qu, Y., Zhang, W., Yu, Y.: Wasserstein distance guided representation learning for domain adaptation. In: AAAI (2018)
- Shwartz-Ziv, R., Armon, A.: Tabular data: Deep learning is not all you need. *Information Fusion* **81**, 84–90 (2022)
- Simonyan, K., Zisserman, A.: Very deep convolutional networks for large-scale image recognition. In: International Conference on Learning Representations (2015)
- Singh, R., Sekhon, A., et al.: Gakco: a fast gapped k-mer string kernel using counting. In: Joint ECML and Knowledge Discovery in Databases. pp. 356–373 (2017)
- Tan, M., Le, Q.: Efficientnet: Rethinking model scaling for convolutional neural networks. In: ICML. pp. 6105–6114. PMLR (2019)
- Whisstock, J.C., Lesk, A.M.: Prediction of protein function from protein sequence and structure. *Quarterly reviews of biophysics* **36**(3), 307–340 (2003)
- Xie, J., Girshick, R., Farhadi, A.: Unsupervised deep embedding for clustering analysis. In: ICML. pp. 478–487 (2016)
- Zou, J., Huss, M., Abid, A., Mohammadi, P., Torkamani, A., Telenti, A.: A primer on deep learning in genomics. *Nature genetics* **51**(1), 12–18 (2019)